

Autoignition of Methyl Valerate at Low to Intermediate Temperatures and Elevated Pressures in a Rapid Compression Machine

Bryan W. Weber^{a,*}, Justin Bunnell^a, Kamal Kumar^b, Chih-Jen Sung^a

^a*Department of Mechanical Engineering, University of Connecticut, Storrs, CT, USA*

^b*Department of Mechanical Engineering, University of Idaho, Moscow, ID, USA*

Abstract

Methyl valerate ($\text{C}_6\text{H}_{12}\text{O}_2$, methyl pentanoate) is a methyl ester and a relevant surrogate component for biodiesel. In this work, we present ignition delays of methyl valerate measured using a rapid compression machine at a range of engine-relevant temperature, pressure, and equivalence ratio conditions. The conditions we have studied include equivalence ratios from 0.25 to 2.0, temperatures between 680 K and 1050 K, and pressures of 15 bar and 30 bar. The ignition delay data demonstrate a negative temperature coefficient region in the temperature range of 720 K–800 K for both $\phi = 2.0$, 15 bar and $\phi = 1.0$, 30 bar, with two-stage ignition apparent over the narrower temperature ranges of 720 K–760 K for the lower pressure and 740 K–760 K at the higher pressure. In addition, the experimental ignition delay data are compared with simulations using an existing chemical kinetic model from the literature. The simulations with the literature model under-predict the data by factors between 2 and 10 over the entire range of the experimental data. To help determine the possible reasons for the discrepancy between simulations and experiments, a new chemical kinetic model is developed using the Reaction Mechanism Generator (RMG) software. The agreement between the experimental data and the RMG model is improved but still not satisfactory. Directions for future improvement of the methyl valerate model are discussed.

*Corresponding Author: bryan.weber@uconn.edu

Keywords: chemical kinetics, rapid compression machine, autoignition, methyl ester

1. Introduction

For transportation applications, biodiesel is an important constituent in improving environmental friendliness of fuels. This is due to its renewability when produced from sustainable agricultural crops and its ability to reduce emissions relative to conventionally fueled engines [1]. Biodiesel typically consists of long-chain methyl ester molecules, with typical compositions of C_{14} to C_{20} [1]. Recognizing that the large molecular size of the methyl esters within biodiesel fuel makes creating and using detailed chemical kinetic mechanisms challenging [2], it is desired to study their combustion chemistry by studying simpler molecules.

A recent review paper summarizes the work on methyl esters relevant to biodiesel combustion [3]; the following summary focuses on ignition delay measurements, since these are the focus of this paper. Autoignition of methyl butanoate (MB, $C_5H_{10}O_2$) has been well-studied in both shock tube and rapid compression machine experiments [4, 5, 6, 7, 8, 9, 10]. The prevalence of MB data in the literature is largely due to the early identification of MB as a potential surrogate fuel for biodiesel [11]. However, the experiments have shown that MB may not be an appropriate surrogate for biodiesel, due to its lack of negative temperature coefficient (NTC) behavior, a requirement for a suitable biodiesel surrogate [3].

Larger methyl esters such as methyl valerate (MV, $C_6H_{12}O_2$, methyl pentanoate) have also been studied as possible biodiesel surrogates. Hadj-Ali et al. [9] used a rapid compression machine (RCM) to study the autoignition of several methyl esters including MV. Although MV exhibited two-stage ignition in this study, little additional research has been done on its oxidation. Korobeinichev et al. [12] studied MV in premixed laminar flames and extended a detailed high temperature chemical kinetic model to include MV and methyl hexanoate.

28 Dmitriev et al. [13] added MV to n-heptane/toluene fuel blends to determine
 29 the resulting intermediate species in premixed flames using a flat burner at
 30 1 atm and an equivalence ratio of 1.75. The addition of MV helped reduce soot
 31 forming intermediates including benzene, cyclopentadienyl, acetylene, propar-
 32 gyl, and vinylacetylene [13]. Hayes and Burgess [14] computationally examined
 33 the peroxy radical isomerization reactions for MV to better understand the low
 34 temperature reaction pathways. Finally, Diévar et al. [15] used diffusion flames
 35 in the counterflow configuration to determine extinction limits for a number of
 36 methyl esters, including MV, and validated a detailed kinetic model with the
 37 experimental data.

38 This work provides additional data for the autoignition of MV. Data is col-
 39 lected in a RCM under engine relevant conditions spanning from 15 bar to 30 bar,
 40 equivalence ratios from 0.25 to 2.0, and temperatures from 682 K to 1048 K. The
 41 NTC region of MV is mapped out to provide additional information on the fi-
 42 delity of using MV as a biodiesel surrogate.

43 **2. Experimental Methods**

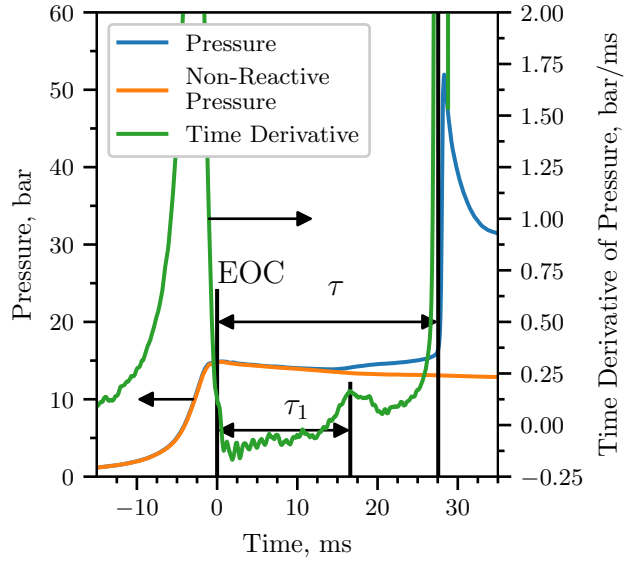
44 The RCM used in this study is a single piston arrangement and is pneu-
 45 matically driven and hydraulically stopped. The device has been described in
 46 detail previously [16] and will be described here briefly for reference. The end
 47 of compression (EOC) temperature and pressure (T_C and P_C respectively), are
 48 independently changed by varying the overall compression ratio, initial pressure
 49 (P_0), and initial temperature (T_0) of the experiments. The piston in the re-
 50 action chamber is machined with a specially designed crevice to suppress the
 51 roll-up vortex effect and promote homogeneous conditions in the reactor during
 52 and after compression [17].

53 The primary diagnostic on the RCM is the in-cylinder pressure measured by
 54 a Kistler 6125C dynamic transducer that is compensated for thermal shock. The
 55 transducer is coupled to a Kistler 5010B charge amplifier. The voltage output
 56 of the charge amplifier is recorded by a National Instruments 9125 analog input

57 device connected to a cDAQ 9178 chassis. The voltage is sampled at a rate
 58 of either 50 kHz or 100 kHz by a LabView VI and processed by a Python
 59 package called UConnRCMPy [18]. Version 3.0.0 of UConnRCMPy [19], 3.6.1
 60 of Python, 2.3.0 of Cantera [20], 1.13 of NumPy [21], 0.19.0 of SciPy [22], and
 61 2.0.1 of Matplotlib [23] were used in the analysis in this paper.

Check this

62 The compression stroke of the RCM brings the fuel/oxidizer mixture to the
 63 EOC conditions, and for suitable thermodynamic states, the mixture will ignite
 64 after a delay period. The definitions of the ignition delays are shown in Fig. 1.
 65 The time of the EOC is defined as the maximum of the pressure trace prior to
 66 the start of ignition and the ignition delays are defined as the time from the EOC
 67 until local maxima in the first time derivative of the pressure. Each experimental
 68 condition is repeated at least five times to ensure repeatability of the data. As
 69 there is some random scatter present in the data, the standard deviation (σ) of
 70 the ignition delays from the runs at a given condition is computed. In all cases,
 71 σ is less than 10 % of the mean value of the overall ignition delay.



72

Figure 1: Definition of the ignition delays used in this work. The experiment in this figure was conducted for a $\phi = 2.0$ mixture with $\text{Ar}/(\text{N}_2 + \text{Ar}) = 0.5$, $P_0 = 0.7806$ bar, $T_0 = 373$ K, $P_C = 14.92$ bar, $T_C = 720$ K, $\tau = (27.56 \pm 0.89)$ ms, $\tau_1 = (16.60 \pm 0.46)$ ms.

In addition to the reactive experiments, non-reactive experiments are conducted to determine the influence of machine-specific behavior on the experimental conditions and permit the calculation of the EOC temperature via the isentropic relations between pressure and temperature [24]. The EOC temperature is calculated by the procedure described in Section 3.

The mixtures considered in this study are shown in Table 1. Four equivalence ratios of MV in “air” are considered. The ratio of Ar : N₂ in the oxidizer is varied to adjust the temperatures reached at the EOC for a given mixture. Two P_C conditions are studied in this work, 15 bar and 30 bar, representing engine-relevant conditions. For the $\phi = 2.0$ condition, only $P_C = 15$ bar is considered because we could not achieve T_C values low enough that the ignition was long enough to be measured in our apparatus (the typical lower limit of ignition delay on the present RCM is approximately 5 ms).

Mixtures are prepared in stainless steel mixing tanks, approximately 17 L and 15 L in size. The proportions of reactants in the mixture are determined by specifying the absolute mass of the fuel, the equivalence ratio (ϕ), and the ratio of Ar : N₂ in the oxidizer. Mixtures are made by first vacuuming the mixing tanks to an ultimate pressure less than 5 torr. Since MV is a liquid with a relatively small vapor pressure at room temperature and pressure, it is measured gravimetrically in a syringe to within 0.01 g of the specified value. The fuel is injected into the mixing tank through a septum. Proportions of O₂, Ar, and N₂ are added manometrically at room temperature and the total pressure is measured by an Omega Engineering MMA type static pressure transducer. The same transducer is used to measure the pressure of the reactants prior to an experiment.

Table 1: Mixtures considered in this work

ϕ	Mole Fraction (purity)				Ar/(N ₂ + Ar)
	MV (100 %)	O ₂ (99.994 %)	Ar (99.999 %)	N ₂ (99.999 %)	
0.25	0.0065	0.2087	0.7848	0.0000	1.0
0.5	0.0130	0.2074	0.7798	0.0000	1.0
1.0	0.0256	0.2047	0.7697	0.0000	1.0
1.0	0.0256	0.2047	0.3849	0.3848	0.5
2.0	0.0499	0.1996	0.0000	0.7505	0.0
2.0	0.0499	0.1996	0.3752	0.3753	0.5

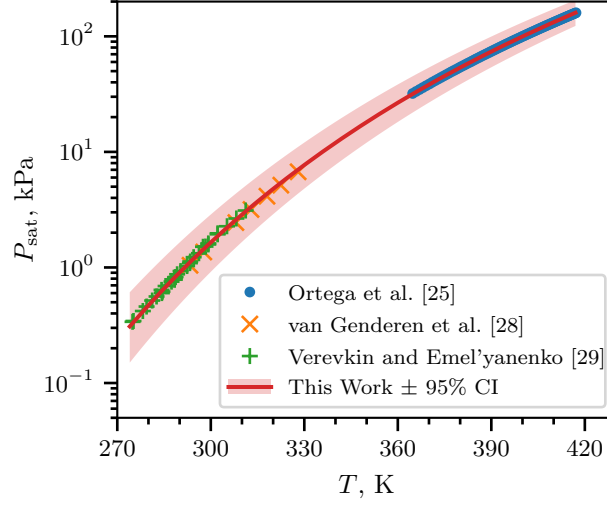
The RCM is equipped with heaters to control the initial temperature of the mixture. After filling in the components to the mixing tanks, the heaters are switched on and the system is allowed 1.5 h to come to steady state. The mixing tanks are also equipped with magnetic stir bars so the reactants are well mixed for the duration of the experiments.

The initial temperature is chosen such that the saturated vapor pressure (P_{sat}) of the fuel at the initial temperature is at least twice the partial pressure of the fuel in the mixing tank. The Antoine equation

$$\log_{10} P_{\text{sat}} = A - \frac{B}{T - C} \quad (1)$$

is used to model the saturated vapor pressure of MV as a function of temperature, where A , B , and C are substance-specific coefficients. Coefficients for Eq. (1) are given in the literature by Ortega et al. [25], Camacho et al. [26], and Stephenson et al. [27]. Unfortunately, the values of the coefficients are different among all three authors and, more importantly, the temperature ranges provided in those three fits do not cover the entire range of interest for this study. Therefore, coefficients for use in Eq. (1) are determined in this work by least squares fitting of the data of Ortega et al. [25], van Genderen et al. [28], and Verevkin and Emel'yanenko [29] using the `curve_fit()` function of SciPy [22] version 0.19.0. Figure 2 shows that the coefficients fit with this procedure give

118 good agreement with the experimental data; values for the coefficients computed
 119 in this work and in the literature works are given in Table 2. The data used to
 120 calculate the coefficients are provided in the Supplementary Material.



121

Figure 2: Saturated vapor pressure of MV as a function of temperature, plotted using the
 122 Antoine equation, Eq. (1), with $A = 6.4030$, $B = 1528.69$, and $C = 52.881$.

Table 2: Antoine Equation coefficients computed in this work and from the literature. The 2σ
 confidence interval is estimated by taking the square root of the diagonals of the covariance
 123 matrix returned from `curve_fit()`

	A	B	C	T_{\min}, K	T_{\max}, K
This Work	6.4030	1528.69	52.881	274.9	417.18
124 2σ Confidence Interval	0.0919	53.47	4.934	—	—
Ortega et al. [25]	6.23175	1429.00	62.30	364.75	417.18
Camacho et al. [26]	5.9644	1281.06	75.94	281	547
Stephenson et al. [27]	6.62646	1658.4	42.09	297	411

125 3. Computational Methods

126 3.1. RCM Modeling

127 The Python 3.6 interface of Cantera [20] version 2.3.0 is used for all sim-
128 ulations in this work. Detailed descriptions of the use of Cantera for these
129 simulations can be found in the work of Weber and Sung [18] and Dames et al.
130 [30]; a brief overview is given here. As mentioned in Section 2, non-reactive
131 experiments are conducted to characterize the machine-specific effects on the
132 experimental conditions in the RCM. This pressure trace is combined with the
133 reactive pressure trace and used to compute a volume trace by assuming that
134 the reactants undergo a reversible, adiabatic, constant composition (i.e., isen-
135 tropic) compression during the compression stroke and an isentropic expansion
136 after the EOC. The volume trace is applied to a simulation conducted in an
137 `IdealGasReactor` in Cantera [20] using the CVODES solver from the SUNDI-
138 ALS suite [31]. The ignition delay from the simulations is defined in the same
139 manner as in the experiments. The time derivative of the pressure in the sim-
140 ulations is computed by second order Lagrange polynomials, as discussed by
141 Chapra and Canale [32].

142 To the best of our knowledge, there are three mechanisms for MV combus-
143 tion available in the literature. The first two, by [12] and [13], were developed
144 to simulate flames, and do not include the low-temperature chemistry necessary
145 to simulate the conditions in these experiments. The third model was devel-
146 oped by [15] and includes low-temperature chemistry of MV, although it was
147 only validated by comparison with flame extinction limits. In converting this
148 mechanism for use in Cantera, we found that there were many species in the
149 thermodynamic database with multiple data entries. For most of these species
150 the thermodynamic data is identical. However, some species are not exact du-
151 plicates. For these species, it is not clear from the thermodynamic database file
152 which data set should be preferred. Since Cantera (and CHEMKIN) choose the
153 first instance of a duplicate species to be used, we retained the first entry for
154 all duplicated species. The detailed [15] model includes 1105 species and 7141

155 reactions, and the CHEMKIN and Cantera formatted input files are available
156 in the Supplementary Material.

157 3.2. Reaction Mechanism Generator

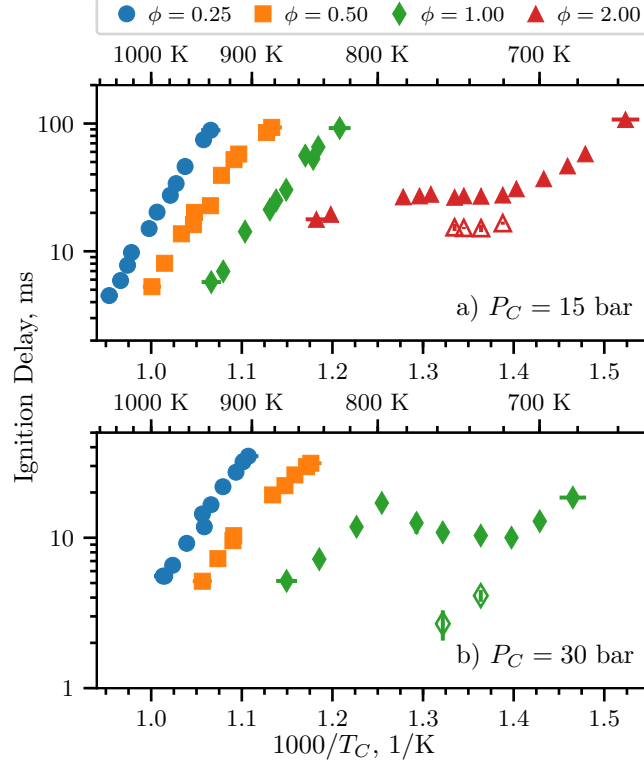
158 In addition to using a mechanism from the literature, we investigate the use
159 of an automatic mechanism generator, the open-source Reaction Mechanism
160 Generator (RMG) [33] version 2.1.0. The Python version of RMG is used,
161 which requires Python 2.7, and version 2.1.0 of the RMG database is used.
162 The final RMG model contains 427 species and 13640 reactions. Note that the
163 number of species is much lower than the Diévert et al. [15] model because
164 the RMG model focuses on only one fuel (MV), but the number of reactions is
165 substantially higher. The input file used to generate the model is available in
166 the Supplementary Material.

167 4. Experimental Results

168 Figure 3 shows the ignition delay results measured in this study. Filled mark-
169 ers denote the overall ignition delay and hollow markers indicate the first-stage
170 ignition delay. Vertical error bars are drawn on the symbols to represent the
171 uncertainty in the ignition delay; for many of the experiments, the uncertainty
172 is approximately the same size as the data point, so the error bar is hidden.
173 Horizontal error bars are shown on the first and last points of each equivalence
174 ratio indicating the estimated uncertainty in the EOC temperature of $\pm 1\%$ [34].
175 Fig. 3a shows the results for a compressed pressure of 15 bar, while Fig. 3b shows
176 the results for a compressed pressure of 30 bar. Note that $\phi = 2.0$ results were
177 not collected for 30 bar, so there are no red data points in Fig. 3b.

178 It can be seen from Fig. 3 that the ignition delays for the $\phi = 0.25$ and 0.5
179 mixtures do not show an NTC region of the ignition delay for both of the
180 pressures studied in this work. However, the $\phi = 1.0$ mixture shows an NTC
181 region at $P_C = 30$ bar between approximately 720 K and 800 K, with measured
182 first-stage ignition delays at 733 K and 757 K. In addition, the $\phi = 2.0$ mixture

183 shows an NTC region of ignition delay at 15 bar from approximately 720 K to
 184 780 K, with measured first-stage ignition delays between 720 K and 750 K.

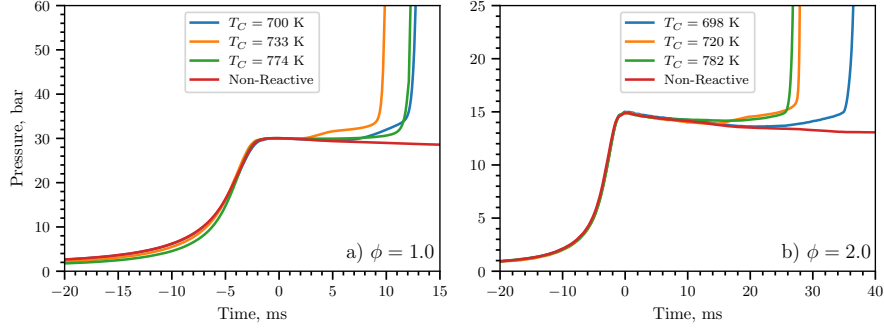


185

Figure 3: Ignition delays of MV as a function of inverse temperature. Filled points are the
 186 overall ignition delays and hollow points are the first stage ignition delays. a) 15 bar. b) 30 bar

187 Figure 4a shows the pressure traces for selected experiments at $\phi = 1.0$, $P_C =$
 188 30 bar. The three reactive pressure traces shown are at the low-temperature end
 189 of the NTC (blue, 700 K), one case with two-stage ignition (orange, 733 K), and
 190 one case near the high-temperature limit of the NTC region (green, 774 K). Also
 191 shown is the non-reactive pressure trace for the 700 K case (red). By comparing
 192 the 700 K pressure trace with the non-reactive pressure trace, it can be seen
 193 that there is substantial heat release prior to main ignition as measured by the
 194 deviation of the reactive pressure trace from the non-reactive trace. However,
 195 there is only one peak in the time derivative of the pressure, so no first-stage
 196 ignition delay is defined for this case. It can also be seen in Fig. 4a that the

197 775 K case shows some heat release prior to ignition, although again there is
 198 only one peak in the time derivative of the pressure. Furthermore, the heat
 199 release at 775 K appears to be more gradual than at the lowest temperature.



200

Figure 4: Selected pressure traces around the NTC region of ignition delay. a) $\phi = 1.0$ b)
 201 $\phi = 2.0$

202 A similar trend can be observed in Fig. 4b for $\phi = 2.0$ at $P_C = 15$ bar,
 203 where pressure traces at several points around the NTC region are plotted. As
 204 in Fig. 4a, the three reactive pressure traces shown are at the low-temperature
 205 end of the NTC (blue, 698 K), one case with two-stage ignition (orange, 720 K),
 206 and one case near the high-temperature limit of the NTC region (green, 782 K).
 207 Also shown is the non-reactive pressure trace for the 698 K case (red). As for
 208 the $\phi = 1.0$ case, the pressure traces show significant heat release prior to the
 209 overall ignition, as judged by deviation from the non-reactive case.

210 5. Computational Results

211 ?? compares experimentally measured overall ignition delays with ignition
 212 delays computed with the detailed model of [15] for the $\phi = 1.0$ experiments.
 213 Results for the other equivalence ratios are similar to these results, so are not
 214 shown here. It is important to note that the model of [15] was not validated
 215 for MV ignition delays, only for extinction strain rates. At 15 bar, the model
 216 tends to under-predict the ignition delay and predicts an NTC region that is not

217 present in the experiments. At 30 bar, the model predicts the low-temperature
218 ignition delays well, but does not predict the NTC region found experimentally.

219 To understand the underlying reasons for the disagreement between the [15]
220 model and the data, we constructed an additional model using RMG (see Sec-
221 tion 3.2). As can be seen in ??, the agreement between the RMG model and
222 the experimental data is similar to the [15] model for the 30 bar data. At 15 bar,
223 the RMG model predicts a somewhat longer ignition delay than the model of
224 [15], but still predicts an NTC region where none is present in the experimental
225 data.

226 In general, there could be three likely sources of error in the models: missing
227 reaction pathways, incorrect values of the reaction rates, and incorrect values
228 for thermodynamic properties of the species. We have noted in Section 3.2 that
229 the RMG model has many more reactions than the [15] model and the algorithm
230 used in RMG considers a substantial number of the possible pathways. This
231 reduces the possibility of missing reaction pathways affecting the model. Further
232 detailed studies are required to ensure that the RMG model includes all of the
233 relevant reaction pathways.

234 The second source of error may be incorrect reaction rate parameters, either
235 because the rates are specified incorrectly in the model (e.g., typos) or because
236 the rates are not well estimated by the typical analogy based-rules. It should
237 be noted that errors of this type may affect the model generated by RMG—if
238 the rates are not estimated correctly, reactions that are important in reality
239 may not be included in the model. Determining the accuracy of the reaction
240 rates used in the RMG and [15] models requires further detailed studies of the
241 models. Another related source of error could be incorrect estimation of the
242 pressure dependence of the reaction rates, which may be particularly important
243 for the isomerization reactions prevalent in low-temperature chemistry.

244 The third source of error may lie in the estimation of the thermodynamic
245 properties of the species, particularly their heats of formation. We have begun to
246 analyze the possibility of this source of error by conducting a reaction pathway
247 analysis to determine which radicals are formed from the breakdown of the fuel.

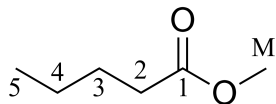


Figure 5: Structure of MV with carbon atoms labeled according to the convention used in Table 3

Table 3: Percent of MV destroyed to form fuel radical species with a hydrogen atom missing at the location indicated in the first column

Radical Site	[15] [%]	RMG Model [%]
2	29.3	7.4
3	17.5	36.0
4	17.5	41.1
5	9.4	3.7
M	26.3	11.8

The following analysis is conducted for a constant volume simulation at 700 K, 30 bar, where the rates of production of the species have been integrated until the time of 20 % fuel consumption. The results of this analysis are shown in Fig. 5 and Table 3 for the two models. The percentages shown in the Table 3 are the percent of the fuel destroyed to form a particular fuel radical by all the reactions that can form that radical.

At the relatively low temperature and high pressure condition of this analysis, all of the fuel is destroyed by H-atom abstractions to form the fuel radicals shown. It can be seen that the two models have quite different distributions of products from the first H-abstraction reactions. The model of [15] predicts that H-abstraction from the second carbon is the most prevalent, followed closely by abstraction from the methyl group. This is in line with the bond energies of the C-H bonds for those carbon atoms; we expect that the presence of the oxygen atoms will cause hydrogen abstraction at the nearby carbons to be favored. However, the RMG model predicts that radicals in the middle of the carbon chain will be primarily formed. The cause of this discrepancy is under investigation, but it may be caused by the estimation of thermodynamic properties of the radicals.

266 6. Conclusions

267 In this study, we have measured ignition delays for methyl valerate over a
268 wide range of engine-relevant pressures, temperatures, and equivalence ratios.
269 An NTC region of the ignition delay and two-stage ignition were recorded for
270 pressures of 15 bar at $\phi = 2.0$ and 30 bar at $\phi = 1.0$. A detailed chemical ki-
271 netic model available in the literature was unable to reproduce the experimental
272 results, so a new model was constructed using the Reaction Mechanism Gen-
273 erator software. Although the new model contains many more reactions than
274 the literature model, it is still unable to predict the experimental ignition de-
275 lays satisfactorily. Possible reasons for the discrepancy include missing reaction
276 pathways, incorrect rate estimates, and incorrect thermodynamic property esti-
277 mates. Future work will include investigation of the discrepancies between mod-
278 els and experiments to further understand the autoignition kinetics of methyl
279 valerate.

280 References

- 281 [1] S. K. Hoekman, C. Robbins, Fuel Processing Technology 96 (2012) 237–249.
- 282 [2] J. Y. Lai, K. C. Lin, A. Violi, Progress in Energy and Combustion Science
283 37 (2011) 1–14.
- 284 [3] L. Coniglio, H. Bennadji, P. Glaude, O. Herbinet, F. Billaud, Progress in
285 Energy and Combustion Science 39 (2013) 340–382.
- 286 [4] W. K. Metcalfe, S. Dooley, H. J. Curran, J. M. Simmie, A. M. El-Nahas,
287 M. V. Navarro, The Journal of Physical Chemistry A 111 (2007) 4001–4014.
- 288 [5] S. M. Walton, M. S. Wooldridge, C. K. Westbrook, Proceedings of the
289 Combustion Institute 32 (2009) 255–262.
- 290 [6] S. Dooley, H. J. Curran, J. M. Simmie, Combustion and Flame 153 (2008)
291 2–32. 16.

- 292 [7] B. Akih-Kumgeh, J. M. Bergthorson, *Energy & Fuels* 24 (2010) 2439–2448.
- 293 [8] B. Akih-Kumgeh, J. M. Bergthorson, *Combustion and Flame* 158 (2011)
294 1037–1048.
- 295 [9] K. Hadj-Ali, M. Crochet, G. Vanhove, M. Ribaucour, R. Minetti, *Proceed-*
296 *ings of the Combustion Institute* 32 (2009) 239–246. 23.
- 297 [10] K. Kumar, C.-J. Sung, *Combustion and Flame* 171 (2016) 1–14.
- 298 [11] E. Fisher, W. J. Pitz, H. J. Curran, C. K. Westbrook, *Proceedings of the*
299 *Combustion Institute* 28 (2000) 1579–1586. 10.
- 300 [12] O. Korobeinichev, I. Gerasimov, D. Knyazkov, A. Shmakov, T. Bolshova,
301 N. Hansen, C. K. Westbrook, G. Dayma, B. Yang, *Zeitschrift für Physikalis-*
302 *che Chemie* 229 (2015).
- 303 [13] A. M. Dmitriev, D. A. Knyazkov, T. A. Bolshova, A. G. Shmakov, O. P.
304 Korobeinichev, *Combustion and Flame* 162 (2015) 1964–1975.
- 305 [14] C. Hayes, D. R. Burgess, *Proceedings of the Combustion Institute* 32 (2009)
306 263–270. 26.
- 307 [15] P. Diévert, S. H. Won, J. Gong, S. Dooley, Y. Ju, *Proceedings of the*
308 *Combustion Institute* 34 (2013) 821–829.
- 309 [16] G. Mittal, C.-J. Sung, *Combustion Science and Technology* 179 (2007) 497–
310 530.
- 311 [17] G. Mittal, C.-J. Sung, *Combustion and Flame* 145 (2006) 160–180.
- 312 [18] B. W. Weber, C.-J. Sung, in: S. Benthall, S. Rostrup (Eds.), *Proceedings*
313 *of the 15th Python in Science Conference*, pp. 36–44.
- 314 [19] B. W. Weber, R. Fang, C.-J. Sung, *UConnRCMPy*, 2017.
- 315 [20] D. G. Goodwin, H. K. Moffat, R. L. Speth, *Cantera: An Object-oriented*
316 *Software Toolkit for Chemical Kinetics, Thermodynamics, and Transport*
317 *Processes*, 2017.

- 318 [21] S. van der Walt, S. C. Colbert, G. Varoquaux, *Computing in Science &*
319 *Engineering* 13 (2011) 22–30.
- 320 [22] E. Jones, T. Oliphant, P. Peterson, others, *SciPy: Open Source Scientific*
321 *Tools for Python*, 2001-.
- 322 [23] J. D. Hunter, *Computing in Science & Engineering* 9 (2007) 90–95.
- 323 [24] D. Lee, S. Hochgreb, *Combustion and Flame* 114 (1998) 531–545.
- 324 [25] J. Ortega, F. Espiau, J. Tojo, J. Canosa, A. Rodríguez, *Journal of Chemical*
325 *& Engineering Data* 48 (2003) 1183–1190.
- 326 [26] A. G. Camacho, J. M. Moll, S. Canzonieri, M. A. Postigo, *Journal of Chem-*
327 *ical & Engineering Data* 52 (2007) 871–875.
- 328 [27] R. M. Stephenson, S. Malanowski, D. Ambrose, *Handbook of the Thermo-*
329 *dynamics of Organic Compounds*, Elsevier, New York, 1987.
- 330 [28] A. C. van Genderen, J. van Miltenburg, J. G. Blok, M. J. van Bommel,
331 P. J. van Ekeren, G. J. van den Berg, H. A. Oonk, *Fluid Phase Equilibria*
332 202 (2002) 109–120.
- 333 [29] S. P. Verevkin, V. N. Emel’yanenko, *Fluid Phase Equilibria* 266 (2008)
334 64–75.
- 335 [30] E. E. Dames, A. S. Rosen, B. W. Weber, C. W. Gao, C.-J. Sung, W. H.
336 Green, *Combustion and Flame* 168 (2016) 310–330.
- 337 [31] A. C. Hindmarsh, P. N. Brown, K. E. Grant, S. L. Lee, R. Serban, D. E.
338 Shumaker, C. S. Woodward, *ACM Transactions on Mathematical Software*
339 31 (2005) 363–396.
- 340 [32] S. C. Chapra, R. P. Canale, *Numerical Methods for Engineers*, McGraw-
341 Hill Higher Education, Boston, 6th ed edition, 2010.
- 342 [33] J. W. Allen, C. F. Goldsmith, W. H. Green, *Physical Chemistry Chemical*
343 *Physics* 14 (2012) 1131–1155.

- ³⁴⁴ [34] B. W. Weber, C.-J. Sung, M. W. Renfro, *Combustion and Flame* 162 (2015)
³⁴⁵ 2518–2528.